NUMERICAL MODELING OF EJECTA DISTRIBUTION AND CRATER FORMATION OF LARGE IMPACT BASINS ON THE MOON.

M. -H. Zhu[1, 2] and K. Wünnemann[1], [1]Museum für Naturkunde, Leibniz Institute for Evolution and Biodiversity Science, Berlin, Germany, Kai.Wuennemann@mfn-berlin.de, [2]Space Science Institute, Macau University of Science and Technology, Macau, mhzhu@must.edu.mo.

Introduction: Large impact basins are the most prominent and oldest landforms on the Moon. Although only a relatively small number of roughly ~ 50-60 basin structures are known, basin-forming impactors clearly dominate over the smaller projectiles in terms of the mass and energy they delivered to the Moon. The impactors penetrate deep into the crust and may even excavate mantle material. They produce large volumes of impact melt and ejecta, which may cover an area with a radius several times larger than the actual basin. Only a few such events may have completely resurfaced the Moon by inverting the crustal stratigraphy, and by emplacing impact melt and originally deep seated crustal or mantle material into the near surface strata. Several attempts have been made to model the formation of impact basins using so-called hydrocodes [e.g. 1-5] using basin morphology and gravity signature as constraint. The ejecta distribution (thickness of the ejecta blanket as a function of distance) has not been considered due to the relatively poor preservation of the ejecta deposits of the old basins that have been modified by impact gardening. However, in a recent study the ejecta distribution at the youngest impact basin, Orientale, has been reconstructed [6] and serves as additional constraint for numerical modeling of basin formation [7]. We present a systamtic study of ejecta distribution at large impact basins as a function of impactor properties (size and velocity) and target properties (crustal thickness and thermal gradient). The goal is to predict the thickness, composition (crustal or mantle material), and melt content of the ejecta blanket as a function of distance.

Modeling: We used the multi-material, multi-rheology 2D iSALE [8,9,10] shock physics code to simulate basin formation. We carried out a suite of impact models: impact velocity: v=10, 20 km s^{-1}; impactor diameter L=50-100 km; crustal thickness h=30, 60 km; thermal gradients according to [1, 2, 3]. The rheological and thermodynamic behavior of the crust and the mantle material is modeled assuming as gabbroic and dunitic composition, respectively. The models consist of the ANEOS equation-of-state for gabbro and dunite, combined with a strength and damage model [10] using parameters according to [1, 11]. We do not consider any effects due to porosity in this work.

For all simulations, we assume a planar target covering an area of 1200 km in lateral and vertical direction with a cell size of 1 km x 1 km in the high-resolution zone. The surface gravitational acceleration

is 1.62 m s^{-2} in all models. All simulations were stopped at 2.5 hours after impact. Due to the axisymmetric nature of the 2D code, all simulations account for vertical impacts only.

According to [1, 2, 3] the thermal gradient in the target is very important for the final structure of the basin. In this work, three thermal gradients (warm, intermediate, and cold) according to [2] were used in the simulations. These temperature profiles represent a range of possible thermal conditions for the Moon during the formation of most basin structures. The warm and intermediate thermal profile have a crust and upper mantle temperature gradient of 10 K/km, and follow the solidus in the upmost 350 km of the mantle and an adiabatic gradient below. The cold temperature profile has a crustal temperature gradient of 10 K/km, mantle temperatures that approach, but do not reach, the solidus between depths of 300-500 km, and a deep mantle temperature of 1750 K.
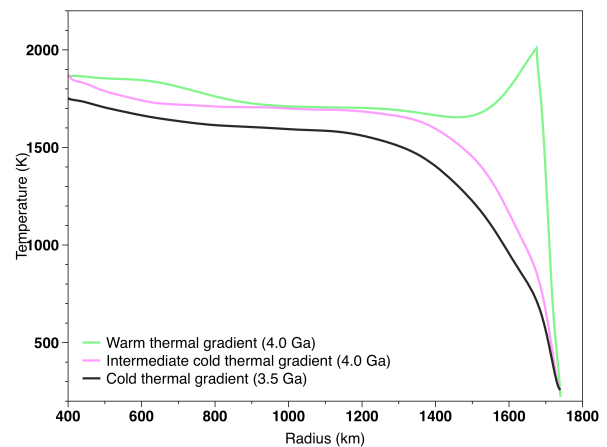

Fig. 1. Three temperature thermal gradients (warm, intermediate, and cold) from [2] were used in this work.

Ejecta Thickness Estimation: We use tracer particles that are initially placed at the center of each computational cell to record the launch angle and velocity at the time of ejection. Assuming pure ballistic flight of the ejecta, we reconstructed the parabolic trajectory of each tracer to calculate its velocity and deposition distance. We assume that each tracer represents the mass of the cell it was initially located in. The surrounding surface of the crater was subdivided into discrete concentric rings. The ejecta thickness was then calculated from the number of tracers that land in each

ring. Note, we do not account for the formation of an ejecta plume in our models and assume that the effect of vaporized material on the distribution of ejecta is negligible in the calculation of ejecta distribution.

Results: Fig. 2 shows the modeled ejecta thickness (L=100 km, v=12 km/s) as a function of distance from basin center for three temperature gradients. In all of the three different impact scenarios the total amount of ejected material is almost the same ($\sim 2.7\times10^6$ km^3). The ejecta thickness decreases proportionally to a power-law with an exponent $e = -3$, which is similar to that derived from the laboratory experiments [12] (see also the companion abstract by *Wünnemann et al.*, "Insight into crater formation, shock metamorphism and ejecta distribution from laboratory experiments and modeling"). It indicates that the power-law function to parameterize the ejecta thickness as a function of distance can be extrapolated from small-scale laboratory experiments to large-scale impact basin. However, the decay exponent of the power-law function differs depending on the thermal gradient. For example, the ejecta deposit is thicker close to the crater rim and decreases more rapidly to a distance of 1400 km (3R) in the case of the warm target ($e = -3.6$) than for the cold target ($e = -3.2$). It is because that the launch angle of most ejecta is > 45° for the warm target but approximately 45° for the cold one. For the same velocity ejecta with a launch angle close to 45° are deposited the furthest whilst shallower or stepper ejection angles results in shorter deposition distances.
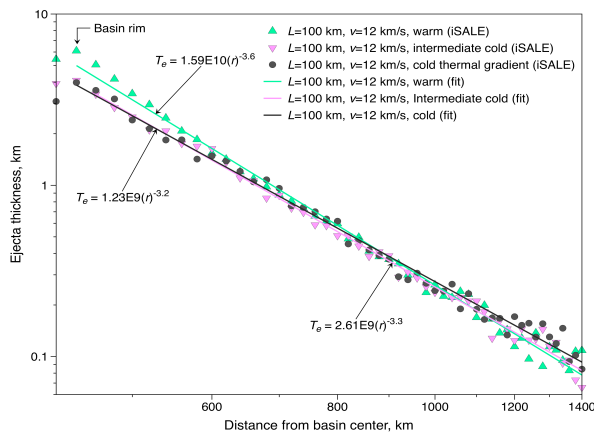

Fig. 2. The ejecta thickness of the vertical impact (L=100 km, v=12 km s^{-1}) on warm, intermediate, and cold target.

The excavation depth is defined as the maximum depth from which material is ejected out of the crater and deposited on the target surface. In our simulations it is independent of the crustal thickness overlying the mantle [7]. Fig. 3 shows the excavation depth against impactor diameter (L=50-100 km) for the three thermal

gradients with an impact velocity of 12 km s^{-1}. The excavation depth increases with increasing size of impactor, almost linearly up to $\sim$50 km depth. For larger impactors the excavation depth grows less strongly. For the warm target, the excavation is in generally 1-3 km deeper than that for the cold target and the difference slightly increases with depth. This indicates that the warmer the material, the softer the target and the easier the impactor can penetrate into the target and excavate material.
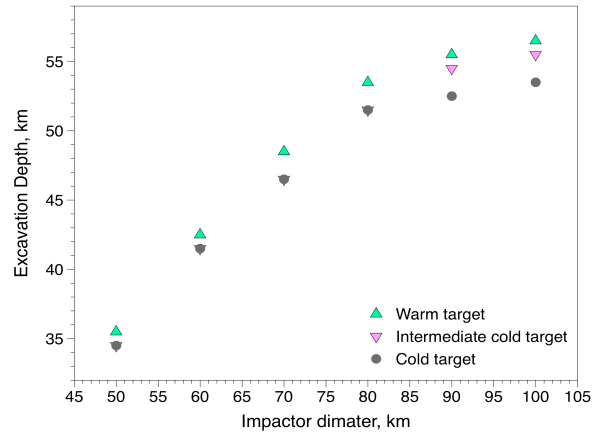

Fig. 3. The excavation depth for the impact event (L=50-100 km, v=12 km s^{-1}) on warm, intermediate, and cold target.

We also determined the melt volume using tracer particles to record the peak shock pressures the material experienced. If the peak shock pressure is in excess of the material's critical shock pressure for melting (gabbro: P_c = 56 GPa; dunite: P_c = 156 GPa) [*e.g.*, 13] the material is considered to be molten. Our results show that the impact-generated melt increases with the size of the impactor (<100 km) for each temperature profile, in agreement with previous estimates and scaling laws [14, 15, 16]. However, for larger impactor, the melt volume deviates significantly from a relatively simple power-law trend [14].

References: [1] Ivanov et al. (2010) *GSA Special Paper,* 465. [2] Miljkovic et al. (2015) *EPSL,* 409. [3] Potter et al. (2013) *JGR,* 118. [4] Potter et al. (2012) *JGR,* 39. [5] Melosh et al., 2013 *Science,* 340. [6] Fassett et al. (2011) *GRL,* 38. [7] Zhu et al. (2015) *LPSC,* Abstract #1832. [8] Amsden et al. (1980) *Los Alamos National Laboratories Report*, LA-8095. [9] Wünnemann et al. (2006) *Icarus*, 180. [10] Collins et al. (2004) *MPS,* 39. [11] Pierazzo et al. (2005) *GSA Special Paper*, 443. [12] Stöffler et al. (1975) *JGR*, 80. [13] Stöffler (1972) *Fortschr. Mineral.*, 49. [14] Marchi et al. (2014) *Nature*, 511. [15] Pierazzo et al. (1997), *Icarus*, 127. [16] Reese et al. (2006) *Icarus*, 184.